Scattering of SH waves around circular canyon in inhomogeneous wedge space

Geophysical Journal International

Geophys. J. Int. (2020) **223,** 45–56
Advance Access publication 2020 July 06
GJI Seismology

doi: 10.1093/gji/ggaa276

Scattering of *SH* waves around circular canyon in inhomogeneous wedge space

Zailin Yang,[1,2] Xinzhu Li,[1] Yunqiu Song,[1] Guanxixi Jiang,[1] Menghan Sun[1] and Xueqian Fang[3]

[1] *College of Aerospace and Civil Engineering, Harbin Engineering University, Harbin, China* 150001. *E-mail: sunmenghan163@sina.com*
[2] *Key Laboratory of Advanced Material of Ship and Mechanics, Ministry of Industry and Information Technology, Harbin Engineering University, Harbin, China* 150001
[3] *State Key Laboratory of Mechanical Behavior and System Safety of Traffic Engineering Structures, Shijiazhuang Tiedao University, Shijiazhuang, China* 050042

Accepted 2020 May 27. Received 2020 April 4; in original form 2019 December 28

SUMMARY

Scattering of *SH* waves around a circular canyon in radial inhomogeneous wedge space is investigated in this paper. Based on the complex function method, the governing equation with variable coefficients is transformed into a standard Helmholtz equation and the corresponding analytical solution to this problem is derived. The unknown coefficients in the wavefield is obtained by enforcing the stress-free condition in the circular canyon, then the incident, reflected and scattering waves in the total wavefield are all acquired. Through the calculation and analysis of the parameters that affect the ground motion, the influence of the circular canyon on the ground motion in the radial inhomogeneous wedge space is obtained. Moreover, combined with graphical results, the effects by inhomogeneous parameter on ground motion with circular canyon in wedge space are conspicuous.

Key words: Earthquake ground motions; Theoretical seismology; Wave propagation; Wave scattering and diffraction.

1 INTRODUCTION

Local topographies, such as canyons, hills, slopes, cliffs and so on, play a significant role in the propagation of seismic wave (e.g. Boore 1972; Marco *et al.* 2014). It is obvious that the influence of local topography on the ground motion subjected to incident seismic wave is crucial to the analysis of seismic surface process (Larose *et al.* 2015). Consequently, the sufficient study on the amplification effect of specific local topography on ground motion has been paid close attention in earthquake engineering.

In recent decades, numerous scholars have investigated the waves scattering of canyons, hills and other local topographies under plane *SH* wave incidence. In the early stage, in order to interpret qualitatively the Pacoima Dam accelerogram during the San Fernando, California, earthquake of 1971 February 9, the influence of semi-circular canyon on the amplitude of surface displacement was analysed (Trifunac 1973). Based on this analytical solution and the wave function expansion method, the research on other sophisticated topography is flourishing, for instance, the semi-elliptical canyon (Wong & Trifunac 1974), the V-shaped canyon (Tsaur & Chang 2008), the circular sectorial canyon (Chang *et al.* 2013), the trapezoidal canyon (Zhang *et al.* 2015) and the deep semi-elliptical canyon with a horizontal edge (Tsaur *et al.* 2018). Furthermore, analytical researches on convex topography were also conducting, the first research on convex topography can date back to the modelling of semi-circular hill on a semi-infinite space (Yuan & Men 1992), then a series of other complicated convex topography were presented by scholars such as the triangular hill (Liu *et al.* 2010), the semi-elliptical hill (Amornwongpaibun & Lee 2013), and the trapezoidal hill (Yang *et al.* 2020). The condition of half-space contained local topography is considered by these researchers. However, due to the surface of some topographies like side slops, cliffs and ridges, which is not in a horizontal plane, it is more appropriate to use wedge space representation (Lee & Sherif 1996; Liu *et al.* 2019).

Nevertheless, a common assumption of these literatures is that the underground medium is homogeneous. The lithologic irregularity intensively affects the characteristics of ground motions, like the long duration ground motion (Motosaka & Mitsuji 2012) and the dynamic stress concentration distribution (Liu *et al.* 2014). Numerical methods are mostly used in the study of seismic motion in an inhomogeneous medium with spatially varying material parameters (Delepine & Semblat 2012; Manolis & Dineva 2015; Ba & Yin 2016). With the continuous development and improvement of computer technology, the numerical approximation method is used to solve the realistic surface configurations. While, the analytical method is still essential because it reveals the physical meaning,

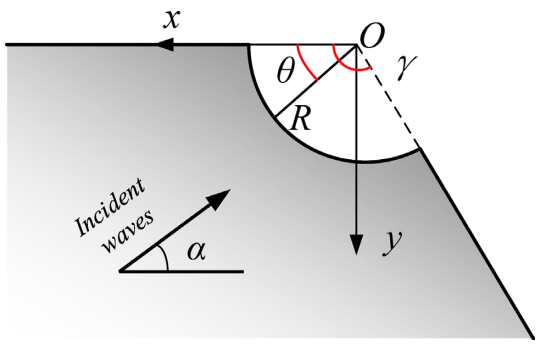

Figure 1. The geometry of the proposed model.

obtains more extensive propagation regular pattern and calibrates the numerical results. Nowadays, some analytical solutions of *SH* waves propagation in inhomogeneous medium has been concerned by scholars. Zhang *et al.* (2017) discussed the soil and topographic effects on ground motion of a surficial inhomogeneous semi-cylindrical canyon of a transfer matrix approach. Jiang *et al.* (2018) illustrate the dynamic response of a shallow circular inclusion under incident *SH* waves in inhomogeneous half-space by applying complex function theory. Zhang *et al.* (2019a,b) used transfer matrix approach to develop an analytical treatments of a cylindrical canyon with a radially piecewise inhomogeneous arbitrary multilayered profile to a finite depth on a homogeneous half-space in terms and the amplification effects of a radially multilayered semi-cylindrical canyon on seismic response of earth and rockfill dam of a radial.

Despite of cliffs and ridges are common on the earth, relevant researches about the scattering problem of them are still scarce (Lee & Sherif 1996; Victor *et al.* 2017; Liu *et al.* 2019). Previous studies considered the lithology as homogeneous, however, the influence of inhomogeneous lithology on ground motion is significant. In the present work, an analytical solution is derived to the scattering problem of a circular canyon in inhomogeneous wedge space, adopting complex function method. The surface on both sides of local topography is not always horizontal. Herewith, wedge space is more sufficient used to understand the influence of local topography in inhomogeneous medium, as the wedge angle changes from 0° to 360° simulating more surface condition. During the process of deriving the analytical solution, the expression of the total wavefields in the wedge space is obtained by truncating the finite term through Fourier series transformation in Section 2. The validity of the proposed analytical solution is proved by comparing the degenerated to homogeneous medium with the existing results in Section 3. Results of steady-state responses with different parameters especially inhomogeneous parameter are presented and discussed in Section 4. Finally, the effects of local topography inhomogeneous medium on ground motion are demonstrated in comparing with homogeneous medium.

2 MODEL AND FORMULATIONS

2.1 The model

The geometry of the proposed model is shown as Fig. 1. The x-axis is at the left edge of the wedge space and is horizontal to the left, the y-axis is vertically down. The origin of the coordinate is located at the centre of the circular arc canyon, and the radius of the canyon is R. The angle of the wedge space is γ, $0 < \gamma \leq 360°$. The incident angle between the incident *SH* wave and the x-axis is α. The variation of the medium density is shown in the following formula

$$\rho(r) = \rho_0 \beta^2 r^{2(\beta-1)}, \quad \beta > 0, \tag{1}$$

where β is the inhomogeneous parameter of the medium, if $\beta > 1$, the density is increased with increase of R. Besides, when $\beta < 1$, the density is decreased with increase of R. When $\beta = 1$, the medium is homogeneous. ρ_0 is the reference mass density.

2.2 The governing equations

For a shear wave velocity c_T, the displacement w with time harmonic satisfies the Helmholtz equation as

$$\nabla^2 w + k^2 w = 0, \tag{2}$$

where $k = \omega/c_T$, $c_T = \sqrt{\mu/\rho}$, k denotes the wave number of *SH* waves, μ is the elastic shear modulus, ω is the circular frequency of the displacement w, and ρ is the mass density of the inhomogeneous medium.

Applying eq. (1), the wave number of *SH* waves in the inhomogeneous medium is expressed as

$$k(r, \theta) = k_0 \cdot \beta r^{\beta-1}. \tag{3}$$

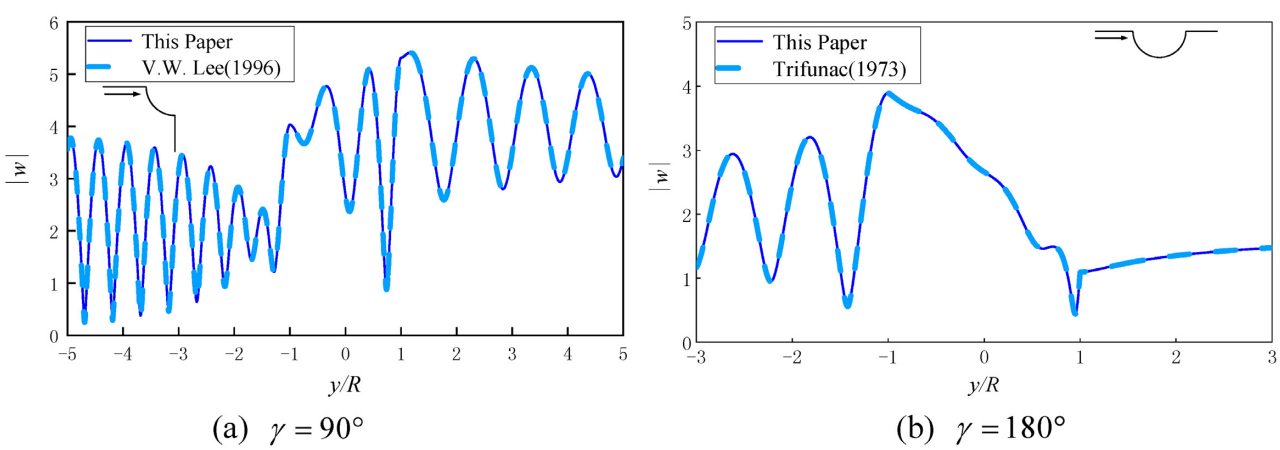

Figure 2. Comparison of degradation calculation and existing results.

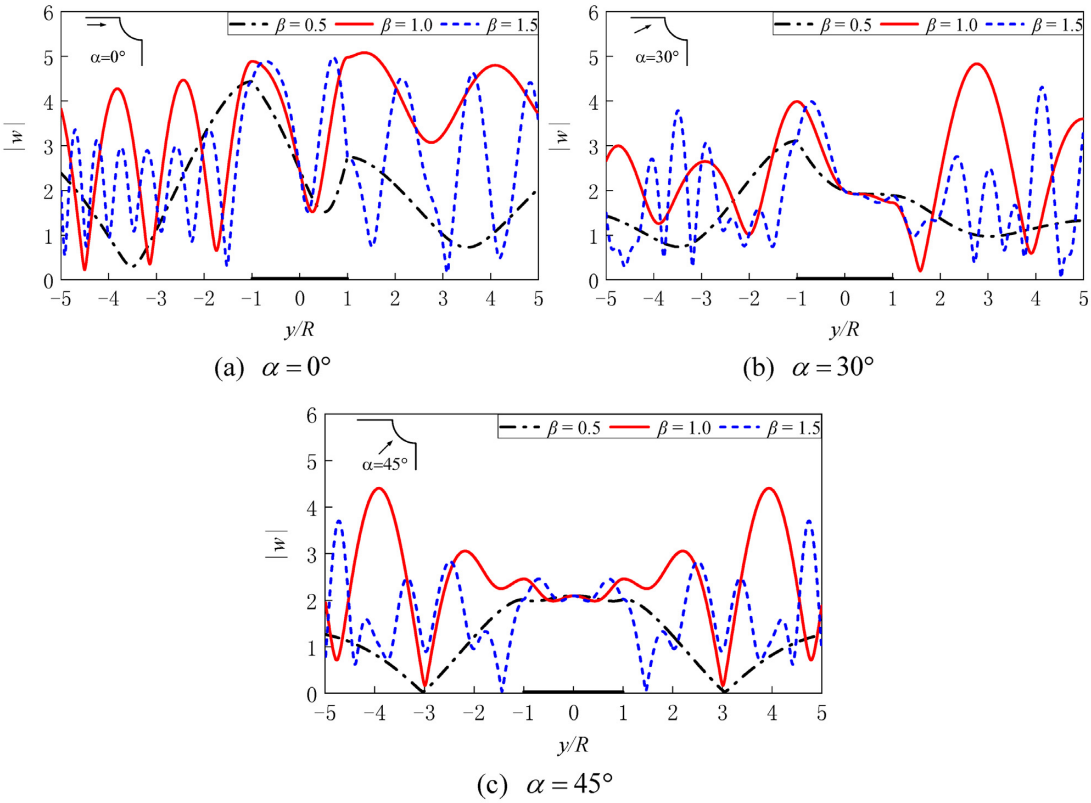

(a) $\alpha = 0°$ (b) $\alpha = 30°$

(c) $\alpha = 45°$

Figure 3. Surface displacement amplitude at three selected inhomogeneous parameters $\beta = 0.5, 1.0, 1.5$, three kinds of incident angles $\alpha = 0°, 30°, 45°$ and wedge angle $\gamma = 90°$ for dimensionless frequency $\eta = 0.75$.

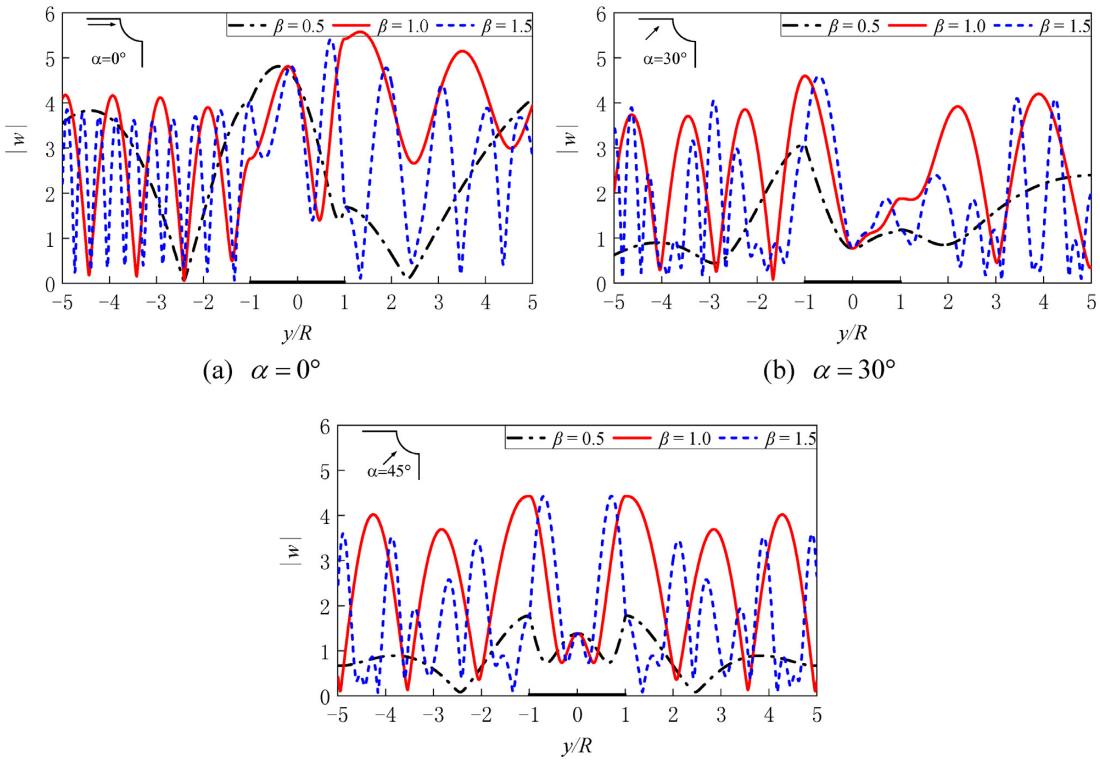

(a) $\alpha = 0°$ (b) $\alpha = 30°$

(c) $\alpha = 45°$

Figure 4. Surface displacement amplitude at three selected inhomogeneous parameters $\beta = 0.5, 1.0, 1.5$, three kinds of incident angles $\alpha = 0°, 30°, 45°$ and wedge angle $\gamma = 90°$ for dimensionless frequency $\eta = 1.0$.

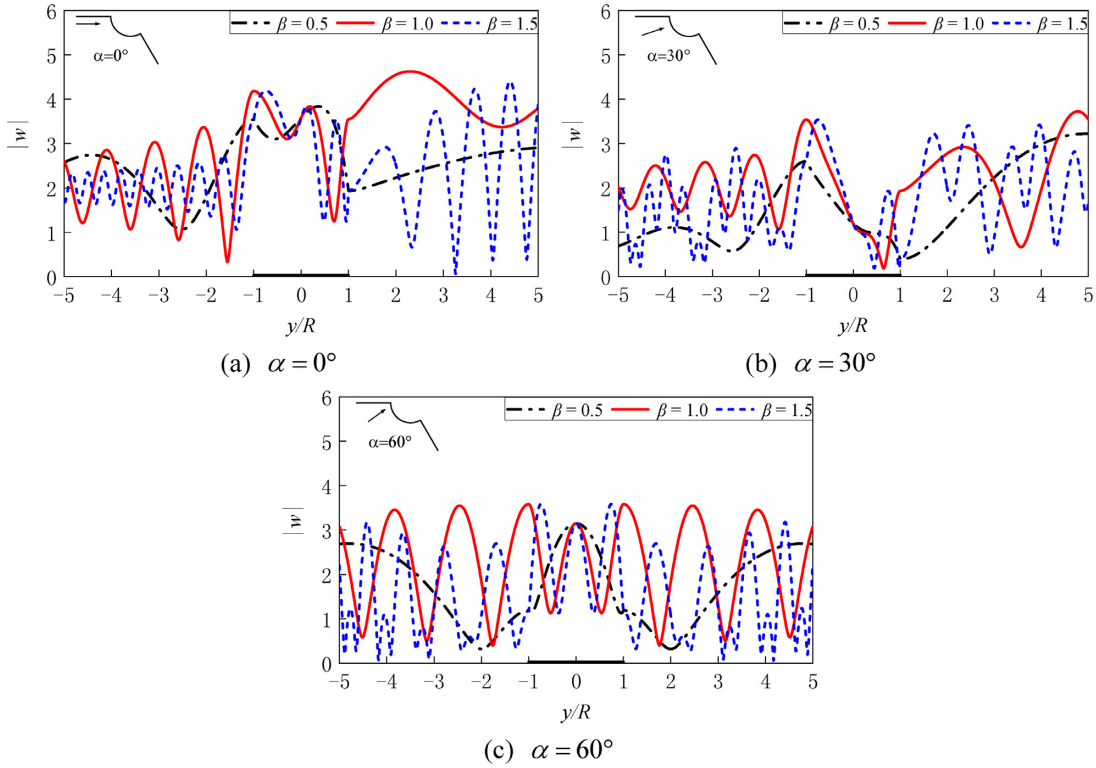

Figure 5. Surface displacement amplitude at three selected inhomogeneous parameters $\beta = 0.5, 1.0, 1.5$, three kinds of incident angles $\alpha = 0°, 30°, 60°$ and dimensionless frequency $\eta = 1.0$ for wedge angle $\gamma = 120°$.

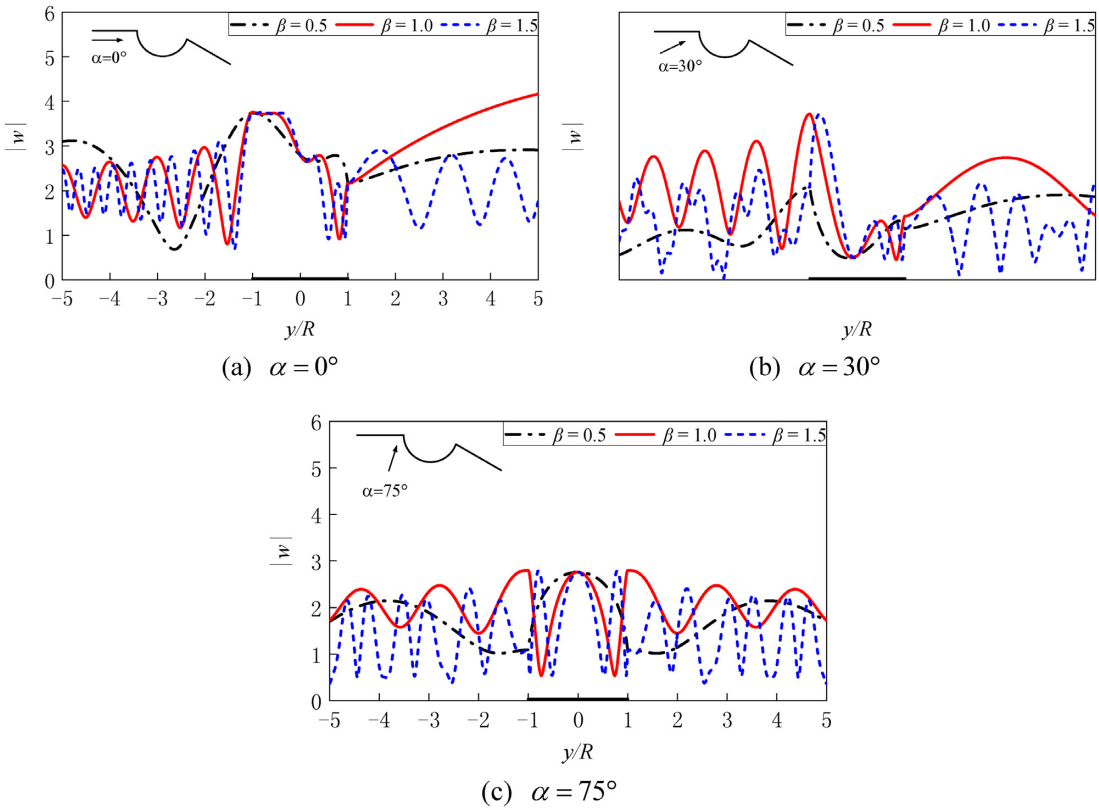

Figure 6. Surface displacement amplitude at three selected inhomogeneous parameters $\beta = 0.5, 1.0, 1.5$, three kinds of incident angles $\alpha = 0°, 30°, 75°$ and dimensionless frequency $\eta = 1.0$ for wedge angle $\gamma = 150°$.

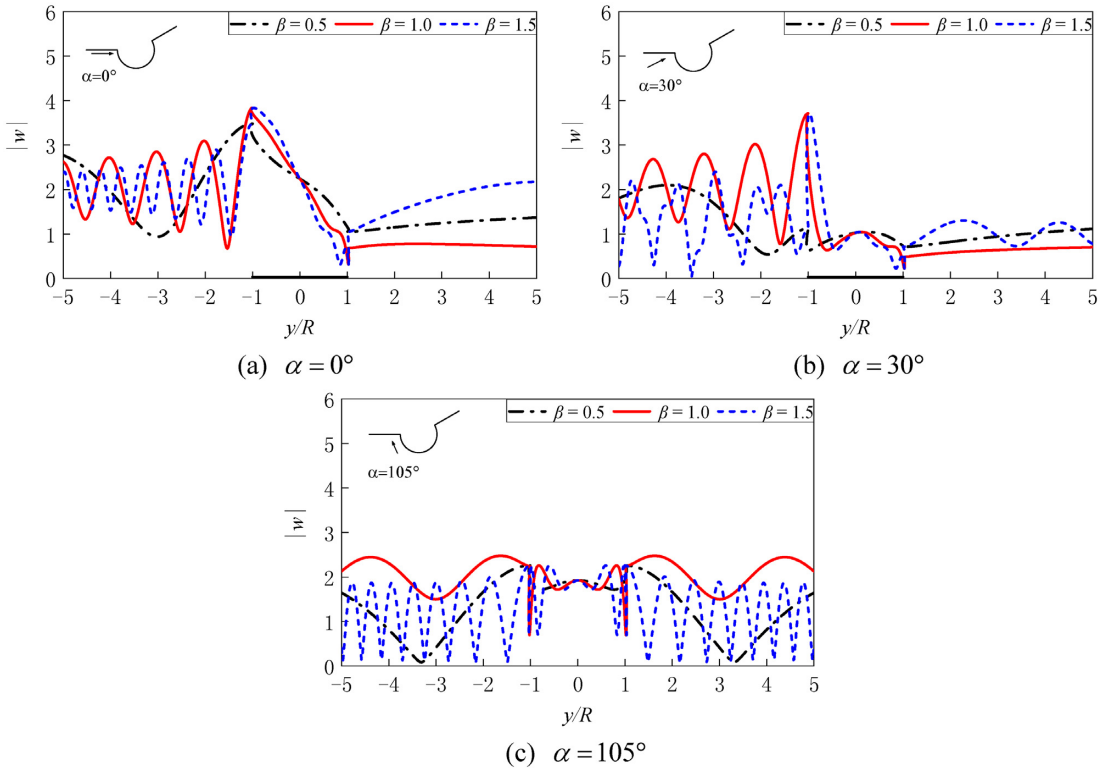

Figure 7. Surface displacement amplitude at three selected inhomogeneous parameters $\beta = 0.5, 1.0, 1.5$, three kinds of incident angles $\alpha = 0^\circ, 30^\circ, 105^\circ$ and dimensionless frequency $\eta = 1.0$ for wedge angle $\gamma = 210^\circ$.

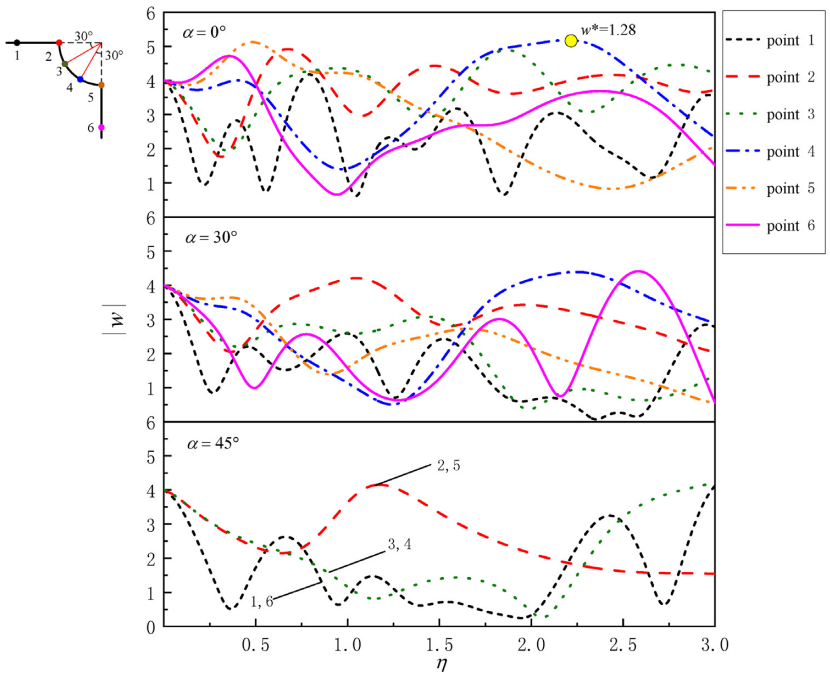

Figure 8. Surface displacement amplitude of six points varied with dimensionless frequency, at $\beta = 1.25$, $\gamma = 90^\circ$ and $\alpha = 0^\circ, 30^\circ, 45^\circ$.

Since the wave number is a function, eq. (2) can be reformulated in the cylindrical coordinate system as

$$r^2 \frac{\partial^2 w}{\partial r^2} + r \frac{\partial w}{\partial r} + \frac{\partial^2 w}{\partial \theta^2} + r^2 k^2 (r, \theta) u = 0. \tag{4}$$

Substituting eq. (3) into eq. (4), the governing equations in the inhomogeneous medium is obtained

$$\frac{\partial^2 w}{\partial r^2} + \frac{1}{r} \frac{\partial w}{\partial r} + \frac{1}{r^2} \frac{\partial^2 w}{\partial \theta^2} + k_0^2 \beta^2 r^{2(\beta-1)} u = 0. \tag{5}$$

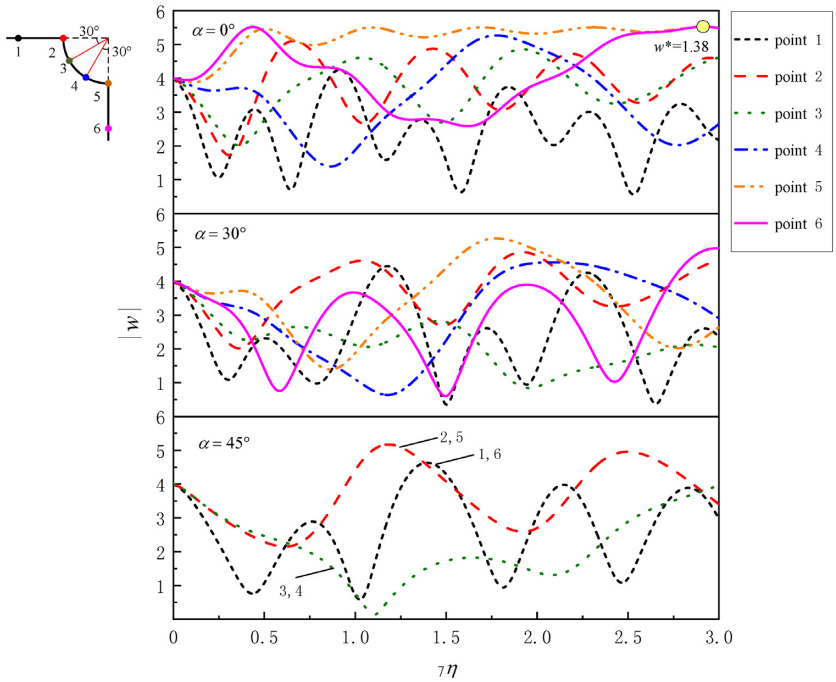

Figure 9. Surface displacement amplitude of six points varied with dimensionless frequency, at $\beta = 1.0$, $\gamma = 90^\circ$ and $\alpha = 0^\circ, 30^\circ, 45^\circ$.

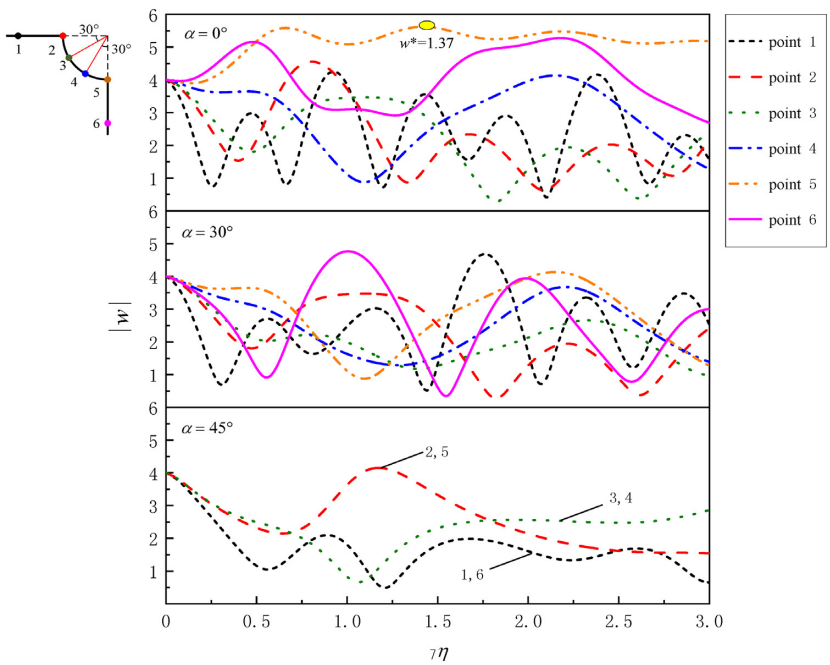

Figure 10. Surface displacement amplitude of six points varied with dimensionless frequency, at $\beta = 0.75, \gamma = 90^\circ$ and $\alpha = 0^\circ, 30^\circ, 45^\circ$.

The partial differential equation with variable coefficient shown in eq. (5) is difficult to be directly solved mathematically. Thus, the complex function method is used firstly, and the complex variable is defined as

$$z = r\mathrm{e}^{\mathrm{i}\theta}. \tag{6}$$

Based on the complex variables, eq. (5) is transformed into

$$\frac{\partial^2 w}{\partial z \partial \bar{z}} + \frac{1}{4}\beta^2 (z\bar{z})^\beta k_0^2 w = 0. \tag{7}$$

Then, in order to gain the standard Helmholtz equation, another pair of variables is utilized to transform eq. (7)

$$\zeta(\xi, \eta) = z^\beta, \bar{\zeta}(\xi, \eta) = \bar{z}^\beta. \tag{8}$$

Finally, the governing equation is rewritten as

$$\frac{\partial^2 w}{\partial \xi^2} + \frac{\partial^2 w}{\partial \eta^2} + \frac{1}{4}k_0^2 w = 0. \tag{9}$$

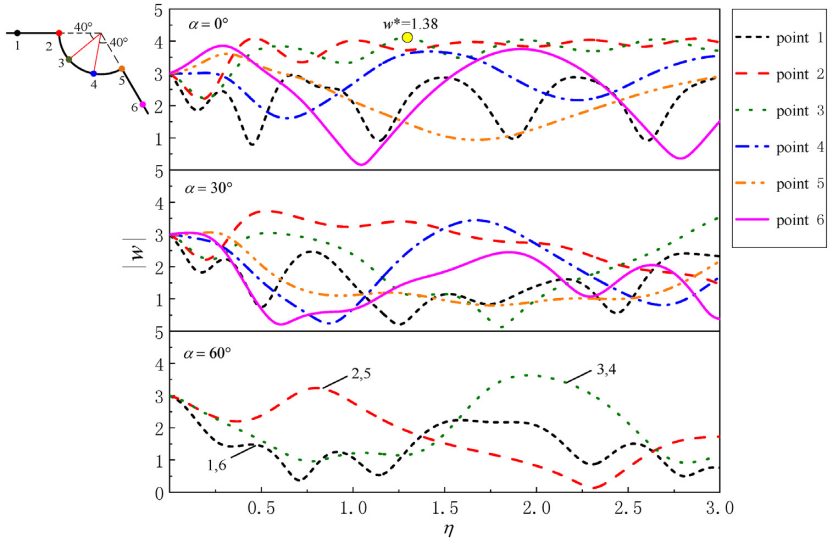

Figure 11. Surface displacement amplitude of six points varied with dimensionless frequency, at $\beta = 1.25, \gamma = 120^\circ$ and $\alpha = 0^\circ, 30^\circ, 60^\circ$.

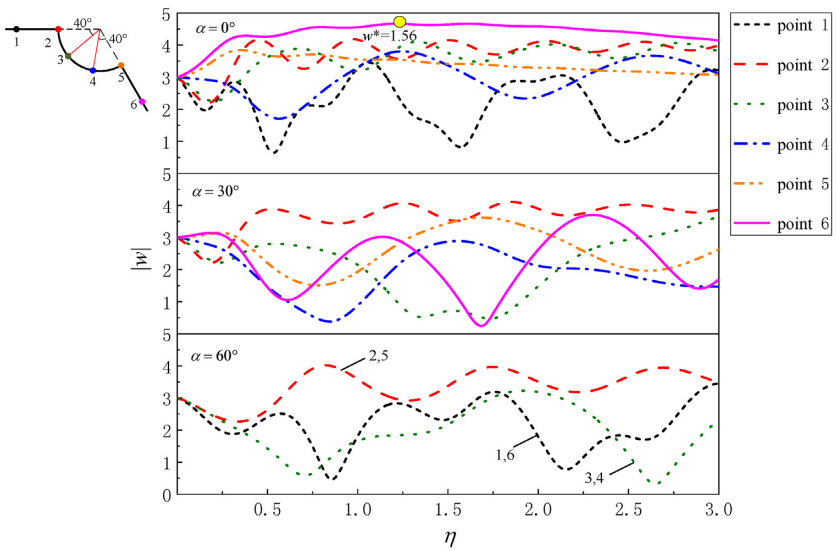

Figure 12. Surface displacement amplitude of six points varied with dimensionless frequency, at $\beta = 1.0, \gamma = 120^\circ$ and $\alpha = 0^\circ, 30^\circ, 60^\circ$.

In accordance with the governing equation, in the ζ plane the corresponding stresses are obtained:

$$\tau_{rz} = \beta\mu\left(\frac{\partial w}{\partial \zeta} z^{\beta-1} \mathrm{e}^{\mathrm{i}\theta} + \frac{\partial w}{\partial \bar{\zeta}} \bar{z}^{\beta-1} \mathrm{e}^{-\mathrm{i}\theta}\right) \tag{10}$$

$$\tau_{\theta z} = \mathrm{i}\beta\mu\left(\frac{\partial w}{\partial \zeta} z^{\beta-1} \mathrm{e}^{\mathrm{i}\theta} - \frac{\partial w}{\partial \bar{\zeta}} \bar{z}^{\beta-1} \mathrm{e}^{-\mathrm{i}\theta}\right). \tag{11}$$

2.3 The total wavefields

The total wavefields w will be written as a sum of the free wavefield $w^{(i+r)}$ and the scattering wavefield $w^{(s)}$:

$$w = w^{(i+r)} + w^{(s)}. \tag{12}$$

The expression of the incident and reflected waves ($w^{(i+r)}$) in the wedge shape in the homogeneous medium proposed by Sanchez-Sesma (1985) is rewritten in the ζ plane, which is expressed as

$$\begin{aligned} w^{(i+r)} &= 2pw_0 J_0(k|\zeta|) + 2pw_0 \sum_{n=1}^{\infty} \mathrm{e}^{-\frac{i2n\pi p}{2}} J_{2np}(k|\zeta|) \\ &\cdot \left[\left(\frac{\zeta}{|\zeta|}\right)^{2np} + \left(\frac{\zeta}{|\zeta|}\right)^{-2np}\right] \cos(2np\alpha) \\ &+ 2pw_0 \sum_{n=0}^{\infty} \mathrm{e}^{-\frac{(2n+1)i\pi p}{2}} J_{(2n+1)p}(k|\zeta|) \\ &\cdot \left[\left(\frac{\zeta}{|\zeta|}\right)^{(2n+1)p} - \left(\frac{\zeta}{|\zeta|}\right)^{-(2n+1)p}\right] \sin((2n+1)\cdot p\alpha), \end{aligned} \tag{13}$$

where p is the fraction factor, $p = \pi/\gamma$, and $J_n(\cdot)$ is the Bessel function of the nth order.

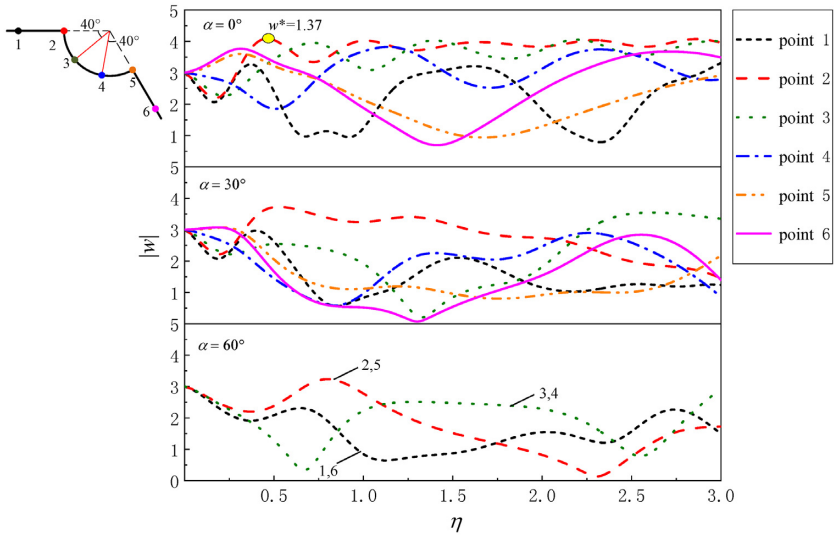

Figure 13. Surface displacement amplitude of six points varied with dimensionless frequency, at $\beta = 0.75, \gamma = 120^\circ$ and $\alpha = 0^\circ, 30^\circ, 60^\circ$.

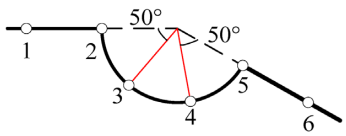

Figure 14. Distribution of six selected points, at $\gamma = 150^\circ$.

The scattering wave generated by the circular canyon topography is shown in the following formula:

$$w^{(s)} = w_0 \sum_{n=0}^{\infty} \left\{ A_n^{(1)} H_{2np}^{(1)}(k|\zeta|) \left[\left(\frac{\zeta}{|\zeta|}\right)^{2np} + \left(\frac{\zeta}{|\zeta|}\right)^{-2np} \right] + A_n^{(2)} H_{(2n+1)p}^{(1)}(k|\zeta|) \left[\left(\frac{\zeta}{|\zeta|}\right)^{(2n+1)p} - \left(\frac{\zeta}{|\zeta|}\right)^{-(2n+1)p} \right] \right\} \tag{14}$$

where $H_n^{(1)}(\cdot)$ is the first kind Hankel function of the nth order, $A_n^{(1)}$ and $A_n^{(2)}$ are the unknown coefficients.

2.4 Boundary conditions

Mathematically, the boundary conditions for the present problem will be expressed as the stress free exists along the entire surface of the wedge space with a circular canyon. The stress-free of the wedge surface are satisfied as

$$\tau_{\theta z} = \tau_{\theta z}^{(i+r)} + \tau_{\theta z}^{(s)} = 0, \theta = 0 \text{ and } \theta = \gamma. \tag{15}$$

Meanwhile, at the circular canyon the boundary condition is

$$\tau_{rz} = \tau_{rz}^{(i+r)} + \tau_{rz}^{(s)} = 0, r = a \tag{16}$$

with $\tau_{rz}^{(i+r)}$ and $\tau_{rz}^{(s)}$ will be obtained by substituting eq. (13) and eq. (14) into eq. (10), respectively.

2.5 The solution of boundary-valued problem

The coefficients $A_n^{(1)}$ and $A_n^{(2)}$ can be determined by using the stress-free boundary condition at the circular canyon as eq. (16). Multiplying eq. (16) with $e^{-im\theta}$ and expanding it into Fourier series of $(0, \gamma)$ yield

$$\begin{cases} \sum_{m=0}^{\infty}\sum_{n=0}^{\infty} A_n^{(1)} \varepsilon_{mn}^{(1)} = -\sum_{m=0}^{\infty}\sum_{n=0}^{\infty} E_{mn}^{(1)} \\ \sum_{m=0}^{\infty}\sum_{n=0}^{\infty} A_n^{(2)} \varepsilon_{mn}^{(2)} = -\sum_{m=0}^{\infty}\sum_{n=0}^{\infty} E_{mn}^{(2)} \end{cases} \tag{17}$$

where

$$\begin{cases} \varepsilon_{mn}^{(1)} = \frac{1}{\gamma}\int_0^{\gamma} \tau_{rz(2m)}^{(s)} e^{-im\theta} d\theta \\ \varepsilon_{mn}^{(2)} = \frac{1}{\gamma}\int_0^{\gamma} \tau_{rz(2m+1)}^{(s)} e^{-im\theta} d\theta \\ F_{mn}^{(1)} = \frac{1}{\gamma}\int_0^{\gamma} \tau_{rz(2m)}^{(i+r)} e^{-im\theta} d\theta \\ F_{mn}^{(2)} = \frac{1}{\gamma}\int_0^{\gamma} \tau_{rz(2m+1)}^{(i+r)} e^{-im\theta} d\theta \end{cases}$$

$\tau_{rz(2m)}^{(s)}$ and $\tau_{rz(2m)}^{(i+r)}$ are the even order of $\tau_{rz}^{(s)}$ and $\tau_{rz}^{(i+r)}$ respectively, $\tau_{rz(2m+1)}^{(s)}$ and $\tau_{rz(2m+1)}^{(i+r)}$ are the odd order of $\tau_{rz}^{(s)}$ and $\tau_{rz}^{(i+r)}$ respectively.

3 METHOD VALIDATION

Before the calculation, several parameters' definitions are introduced. β is inhomogeneous parameter defined in eq. (1). Moreover, the dimensionless frequency η can be formulated as

$$\eta = 2R/\lambda = kR/\pi \tag{18}$$

and the last parameter is the surface displacement amplitude $|w|$

$$|w| = \sqrt{\mathrm{Re}^2(w) + \mathrm{Im}^2(w)} \tag{19}$$

where $\mathrm{Re}(\cdot)$ and $\mathrm{Im}(\cdot)$ denote the real and imaginary parts of a complex variable.

In order to verify the validity of the method proposed this paper, the comparisons with the published results (Trifunac 1973; Lee & Sherif 1996) are shown in Figs 2(a) and (b). The displacement at the condition of inhomogeneous parameter $\beta = 1$, the dimensionless frequency $\eta = 2$ and the wedge angle $\gamma = 90^\circ$ for this method are described by the solid line in Fig. 2(a), meanwhile the displacement at the condition of $\beta = 1$, $\eta = 1.25$ and $\gamma = 180^\circ$ for the present method are shown by the solid line in Fig. 2(b). The numerical results in Fig. 2 shows that the present method is in well agreement with the published results, which can verify the validity of the present method.

Table 1. Calculated results of the displacement amplification factor w^* for six observer points at $\gamma = 150°$, $\beta = 1.25$ and $\alpha = 0°, 30°, 75°$.

		w^*														
	α				$0°$						$30°$				$75°$	
β	Point η	1	2	3	4	5	6	1	2	3	4	5	6	1, 6	2, 5	3, 4
1.25	0.001	1.00	1.00	1.00	1.00	1.00	1.00	1.00	1.00	1.00	1.00	1.00	1.00	1.00	1.00	1.00
	0.5	0.67	1.42	1.45	0.64	0.85	0.92	0.37	1.39	1.20	0.37	0.55	0.34	0.53	1.06	0.44
	1.0	0.78	1.55	1.56	1.08	0.43	0.50	0.58	1.36	0.67	0.54	0.24	0.37	0.66	0.62	0.68
	1.5	1.25	1.60	1.58	0.85	0.35	0.84	0.34	1.17	0.19	0.81	0.35	0.63	0.61	0.25	1.23
	2.0	0.69	1.62	1.59	0.86	0.57	1.23	0.89	0.89	0.83	0.77	0.58	0.31	0.11	0.60	0.46
	2.5	0.74	1.64	1.60	0.96	0.69	1.23	0.57	0.53	1.33	0.57	0.51	0.25	0.62	0.99	0.85
	3.0	1.25	**1.66**	1.60	0.77	0.65	0.88	0.89	0.13	**1.50**	0.51	0.64	0.98	0.64	**1.30**	1.14

Table 2. Calculated results of the displacement amplification factor w^* for six observer points at $\gamma = 150°$, $\beta = 1.0$ and $\alpha = 0°, 30°, 75°$.

		w^*														
	α				$0°$						$30°$				$75°$	
β	Point η	1	2	3	4	5	6	1	2	3	4	5	6	1, 6	2, 5	3, 4
1.0	0.001	1.00	1.00	1.00	1.00	1.00	1.00	1.00	1.00	1.00	1.00	1.00	1.00	1.00	1.00	1.00
	0.5	0.46	1.41	1.45	0.75	1.04	1.19	0.51	1.43	1.13	0.41	0.66	0.67	1.17	1.27	0.34
	1.0	1.24	1.57	1.54	1.16	0.90	1.18	1.23	1.55	0.49	0.54	0.60	0.93	0.60	1.16	0.86
	1.5	0.41	1.65	1.54	0.85	0.79	1.16	0.69	1.58	0.38	0.73	0.89	1.23	0.98	1.32	1.04
	2.0	1.30	**1.66**	1.54	1.08	0.71	1.15	1.10	1.59	1.03	1.02	0.78	0.86	1.19	**1.37**	0.48
	2.5	0.36	1.64	1.54	0.90	0.65	1.13	0.93	1.61	1.43	0.49	0.52	0.80	0.78	1.30	1.14
	3.0	1.32	1.64	1.55	1.02	0.60	1.13	0.87	**1.62**	1.35	0.65	0.63	1.06	0.44	1.36	0.68

Table 3. Calculated results of the displacement amplification factor w^* for six observer points at$\gamma = 150°$,$\beta = 0.75$ and $\alpha = 0°, 30°, 75°$.

		w^*														
	α				$0°$						$30°$				$75°$	
β	Point η	1	2	3	4	5	6	1	2	3	4	5	6	1, 6	2, 5	3, 4
0.75	0.001	1.00	1.00	1.00	1.00	1.00	1.00	1.00	1.00	1.00	1.00	1.00	1.00	1.00	1.00	1.00
	0.5	0.83	1.42	1.43	0.89	0.85	0.90	0.89	1.39	1.06	0.49	0.55	0.51	0.95	1.06	0.31
	1.0	0.60	1.55	1.48	1.15	0.43	0.49	0.19	1.36	0.34	0.48	0.24	0.22	0.25	0.62	0.99
	1.5	1.34	1.60	1.45	1.02	0.35	0.55	0.61	1.17	0.53	0.85	0.35	0.54	0.80	0.25	0.79
	2.0	0.84	1.62	1.46	1.11	0.57	0.90	0.32	0.89	1.18	1.07	0.58	0.64	0.84	0.60	0.74
	2.5	0.62	1.63	1.50	1.06	0.68	1.08	0.73	0.52	**1.42**	0.52	0.52	0.50	0.62	0.99	1.06
	3.0	1.25	**1.68**	1.52	1.06	0.62	0.92	0.72	0.14	1.03	0.62	0.66	0.42	0.15	**1.27**	0.65

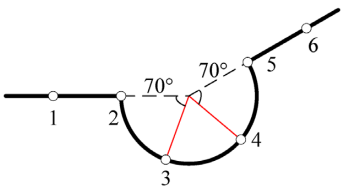

Figure 15. Distribution of six selected points, at $\gamma = 210°$.

4 NUMERICAL DISCUSSION

It is indicated by some parametric studies that the propagation of seismic wave is mainly affected by geometry of the local topography, medium property, wavelength and incident wave angle. For this work, four parameters are mainly discussed, namely the inhomogeneous parameter, dimensionless frequency, incident wave angle and wedge angle.

The present work primarily explores the influence of inhomogeneous medium on the displacement amplitudes. Hence, Figs 3(a)–(c) show the surface displacement amplitude at different incident angle ($\alpha = 0°$, $\alpha = 30°$ and $\alpha = 45°$) of the dimensionless frequency $\eta = 0.75$, the vertex angle $\gamma = \pi/2$ and the inhomogeneous parameter $\beta = 0.5, 1.0, 1.5$. In the figures, the horizontal axis represents the position of the surface, $-1 \leq y/R \leq 1$ is the circular canyon, $-5 \leq y/R < -1$ and $1 < y/R \leq 5$ are the surface position of the wedge, and the vertical axis represents the surface displacement amplitude. By means of this figure, the surface displacement amplitude at the same incident angle increased with the increases of inhomogeneous parameter, but the displacement in inhomogeneous medium are almost smaller than that in homogeneous medium, which is shown by the red curve in Fig. 2. In Fig. 3, it can be seen that the position where the maximum displacement amplitude occurs moves from $y/R = \pm 1$ (the interface between the circular canyon and the surface) to the surface when the incident angle varied from horizontal to 45°. However, if the inhomogeneous parameter $\beta < 1$, the maximum displacement always appears near the point of $y/R = \pm 1$. Concurrently, when the incident angle varied from horizontal to oblique, the influence of inhomogeneous parameter on surface displacement increases substantially.

To give a clear portrait of the dimensionless frequency influences on surface motions, we increase the dimensionless frequency to 1.0 to calculate the displacement under the same condition as in Fig. 3, the calculated results are shown in Fig. 4. It is obvious that when dimensionless frequency increases, the displacement fluctuates more intensely. Meanwhile, in the case of oblique incidence, the surface displacement amplitude increases evidently when inhomogeneous parameter rises. The maximum value point of displacement amplitude moves from both sides to the interface between the canyon and surface in symmetrical incident, through comparing with Fig. 3(c).

Table 4. Calculated results of the displacement amplification factor w^* for six observer points at $\gamma = 210°$, $\beta = 1.25$ and $\alpha = 0°, 30°, 105°$.

		w^*														
	α	0°						30°						105°		
β	Point η	1	2	3	4	5	6	1	2	3	4	5	6	1, 6	2, 5	3, 4
1.25	0.001	1.00	1.00	1.00	1.00	1.00	1.00	1.00	1.00	1.00	1.00	1.00	1.00	1.00	1.00	1.00
	0.5	0.74	2.05	1.78	0.71	0.42	0.46	0.31	**1.86**	1.30	0.44	0.29	0.30	0.24	0.88	0.83
	1.0	1.27	2.17	1.94	0.64	0.22	0.27	0.44	1.64	0.44	0.42	0.15	0.27	1.09	0.44	1.23
	1.5	1.67	2.23	1.99	0.59	0.30	0.38	1.02	1.12	0.97	0.66	0.35	0.54	0.19	1.00	1.04
	2.0	0.66	2.26	2.03	0.49	0.29	0.40	1.36	0.45	1.77	0.54	0.33	0.53	1.12	1.28	1.16
	2.5	1.43	2.27	2.07	0.49	0.20	0.30	0.43	0.33	1.81	0.39	0.17	0.32	0.43	1.01	1.11
	3.0	1.59	**2.29**	2.09	0.42	0.13	0.21	0.16	1.05	1.07	0.43	0.14	0.34	**1.42**	0.58	1.11

Table 5. Calculated results of the displacement amplification factor w^* for six observer points at $\gamma = 210°$, $\beta = 1.0$ and $\alpha = 0°, 30°, 105°$.

		w^*														
	α	0°						30°						105°		
β	Point η	1	2	3	4	5	6	1	2	3	4	5	6	1, 6	2, 5	3, 4
1.0	0.001	1.00	1.00	1.00	1.00	1.00	1.00	1.00	1.00	1.00	1.00	1.00	1.00	1.00	1.00	1.00
	0.5	0.62	2.11	1.68	0.86	0.57	0.60	0.80	2.04	1.16	0.53	0.40	0.43	**1.42**	1.30	1.00
	1.0	1.80	2.23	1.84	0.70	0.40	0.45	1.66	2.16	0.37	0.44	0.28	0.34	1.36	1.30	1.08
	1.5	0.52	2.27	1.89	0.71	0.30	0.37	0.98	2.22	1.20	0.78	0.35	0.45	1.16	1.29	1.26
	2.0	1.82	2.29	1.92	0.62	0.24	0.31	1.50	2.25	1.77	0.66	0.28	0.38	0.92	1.27	0.99
	2.5	0.50	2.30	1.95	0.57	0.20	0.27	1.28	2.26	1.48	0.43	0.17	0.25	0.82	1.25	1.23
	3.0	1.83	**2.31**	1.97	0.56	0.17	0.24	1.22	**2.28**	0.58	0.56	0.18	0.27	0.95	1.24	1.07

Table 6. Calculated results of the displacement amplification factor w^* for six observer points at $\gamma = 210°$, $\beta = 0.75$ and $\alpha = 0°, 30°, 105°$

		w^*														
	α	0°						30°						105°		
β	Point η	1	2	3	4	5	6	1	2	3	4	5	6	1, 6	2, 5	3, 4
0.75	0.001	1.00	1.00	1.00	1.00	1.00	1.00	1.00	1.00	1.00	1.00	1.00	1.00	1.00	1.00	1.00
	0.5	1.33	2.05	1.58	1.00	0.42	0.44	1.25	1.86	1.04	0.61	0.29	0.30	0.72	0.88	1.14
	1.0	0.71	2.17	1.70	0.84	0.22	0.25	0.17	1.63	0.42	0.50	0.15	0.20	0.50	0.44	1.00
	1.5	1.84	2.26	1.76	0.79	0.32	0.37	0.46	1.14	1.30	0.84	0.33	0.44	0.93	0.98	1.26
	2.0	1.36	2.23	1.75	0.78	0.30	0.55	0.58	0.56	1.71	0.78	0.33	0.28	0.36	1.19	1.08
	2.5	1.85	1.62	1.95	0.92	0.41	0.73	1.90	0.80	1.06	0.47	0.53	0.75	0.96	1.01	1.15
	3.0	1.19	**2.76**	1.76	0.82	0.68	2.04	**2.07**	1.76	0.84	0.75	0.59	1.80	**1.61**	0.89	1.15

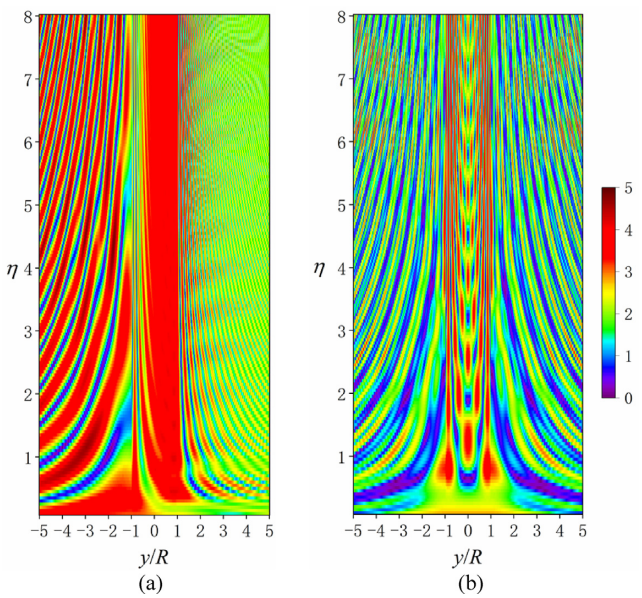

Figure 16. Spectral variations in surface displacement amplitude around the circular canyon with $\beta = 1.25$ and $\gamma = 120°$ at $\alpha = 0°, 60°$.

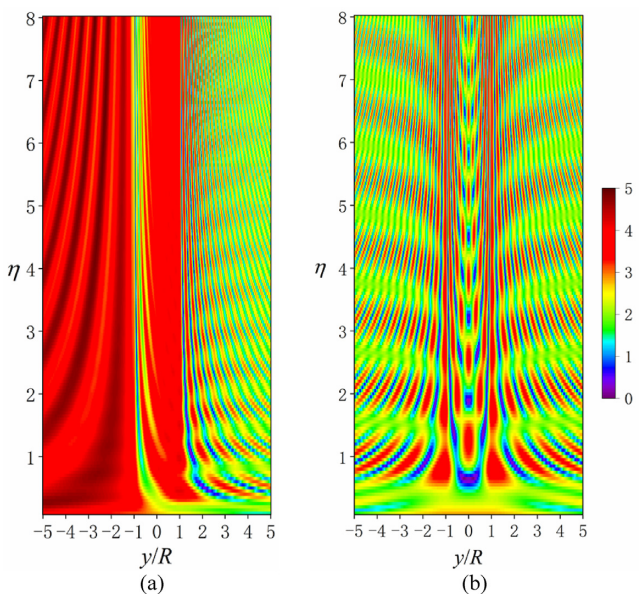

Figure 17. Spectral variations in surface displacement amplitude around the circular canyon with $\beta = 1.0$ and $\gamma = 120°$ at $\alpha = 0°, 60°$.

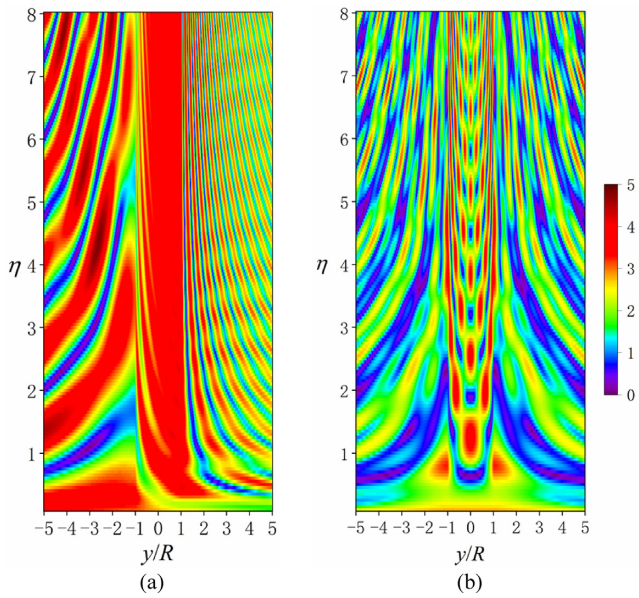

Figure 18. Spectral variations in surface displacement amplitude around the circular canyon with $\beta = 0.75$ and $\gamma = 120^\circ$ at $\alpha = 0^\circ, 60^\circ$.

It implies that different inhomogeneous parameters are sensitive to the variation of dimensionless frequency and incident angle.

Obviously, it is necessary to consider the influence of different wedge angle on surface displacement. Therefore, Figs 5–7 reveal the displacement amplitude with wedge angles of 120°, 150° and 210° respectively. The parameters are set as $\eta = 1.0$, $\beta = 0.5, 1.0, 1.5$ and incident angles are horizontal ($\alpha = 0^\circ$), oblique (α=30°) and symmetrical ($\alpha=\gamma/2$). Compared with different wedge angles by means of Figs 4–7, it can be found out that when wedge angle increases, the maximum displacement amplitude tends to decrease obviously. The maximum surface displacement amplitude of the wedge angle is 210° decreases by 70 per cent compared with the right-angle wedge. When $\gamma = 90^\circ$, compared with other wedge angles, the surface displacement amplitude on the right side of the circular canyon have a significant increase.

Additionally, the local topography also has a remarkable impact on the scattering of *SH* waves. Thus, in the research process of this paper, to investigate the amplification effect of circular canyon on surface displacement amplitude in inhomogeneous medium, the following graphical results are analysed. Here, in order to presenting the degree of displacement amplification of the canyon, another parameter named displacement amplification factor (w^*) is defined:

$$w^* = \frac{|w|}{\bar{w}}, \tag{19}$$

where $\bar{w}$ is the surface displacement amplitude under the quasi-static condition.

First, six representative observer points are selected in this part and illustrated in each figure. The inhomogeneous parameters equal to 1.25, 1.0, and 0.75 respectively and the incident angles are $\alpha = 0^\circ, 30^\circ, 45^\circ$ in the subfigure. In Figs 8–10, it is perceived that when $\gamma = 90^\circ$, the canyon has the strongest amplification effect on the displacement amplitude at point 5. By means of the calculated results, the maximum value of w^* is 1.28 and occurs at the inhomogeneous parameter equals to 1.0. Nevertheless, when medium is inhomogeneous ($\beta = 1.25$ and 0.75), the amplification effect of the canyon is weakened as shown in Fig. 9, especially when the inhomogeneous parameter is greater than 1.

Secondly, the angle of the wedge space is increased to 120° in calculation, and the results are represented in Figs 11–13. Obviously, when wedge angle increases, the displacements amplitude decreases generally. However, it can be found that the amplification effect of the circular canyon on the displacement amplitude increases and the amplification effect is about 1.6 times. Similarly, the maximum displacement amplification factor occurs at the condition of inhomogeneous parameter equals to 1.0 as well. Meanwhile, the amplification is still weakened in inhomogeneous medium. In addition, the maximum amplification effect of the canyon appears at point 2 and point 3 when the medium is inhomogeneous, and at point 6 when the medium is homogeneous.

Thirdly, the case of the wedge space angle equals to 150° is calculated. For purpose of representing the amplification effect of circular canyon on ground motion more directly, the results of this example are given by displacement amplification factor. Six observer positions are selected as shown in Fig. 14. Tables 1–3 present the displacement amplification factor with dimensionless frequency varies, corresponding to $\beta = 1.25, 1.0, 0.75$ respectively. The maximum displacement amplification factor ω^*_{max} at various incident angles is expressed in bold. Currently, the amplification effect of the circular canyon on the surface displacement amplitude is about 1.7 times. Based on the graphical results of different wedge angles, the amplification coefficient of the circular canyon increases with the increase of the wedge angle. That may because during the interaction between the angle of wedge and the existence of the canyon, the amplification effect by the canyon on the surface displacement is more significant than the energy absorption by the increase of wedge angle. However, the amplification effect of the circular canyon on the surface displacement amplitude decreases with the increase of inhomogeneous parameters.

Finally, the condition of the wedge angle equals to 210° is considered. Fig. 15shows the cross section and six positions on the ground surface. Similarly, Tables 4–6 demonstrate the displacement amplification factor with dimensionless frequency variation, corresponding to $\beta = 1.25, 1.0, 0.75$ respectively. Combined with the data in three tables, the displacement amplification factor increases to 2.76. Meanwhile, the maximum amplification effect of topography on surface displacement occurs at the inhomogeneous parameter equals to 0.75, same as the condition of wedge angle equals to 150°. Association with the analysis of the last group of examples, the amplification effect of circular topography in inhomogeneous wedge is still weakening, but the amplification effect will increase sharply at some conditions.

In order to directly observe the surface displacement amplitude changes around the local circular canyon topography in the inhomogeneous wedge space, the surface displacement spectrums are illustrated in Figs 16–18 with the frequency varied is given below. Figs 16(a), 17(a) and 18(a) correspond to $\beta = 1.25$, $\beta = 1.0$ and $\beta = 0.75$, respectively under horizontal incidence ($\alpha = 0^\circ$). Similarly, Figs 16(b), 17(b) and 18(b) correspond to $\beta = 1.25$, $\beta = 1.0$ and $\beta = 0.75$, respectively under oblique incidence ($\alpha = 60^\circ$). Combing with these figures, one obvious phenomenon is found out that inhomogeneous medium is beneficial to reduce the amplification effect of circular canyon on surface displacement amplitude. For horizontal incident *SH* wave, the reduce effect is mainly reflected in the illuminated side, while for oblique incidence cases, it is on both sides. When the wedge space is inhomogeneous, the amplitude of surface displacement is more sensitive to the variation of dimensionless frequency.

5 CONCLUSION

In this paper, an analytical solution for *SH* waves scattering by a circular canyon in inhomogeneous wedge space has been addressed by using complex function method. Comparing with the existing results (Lee *et al.*1996; Trifunac 1973), the validity of the proposed analytical solution is verified. To demonstrate the amplification of ground motion of the inhomogeneous wedge space with a circular canyon, the surface displacement amplitude under different inhomogeneous parameters is calculated and discussed. According to the analysis of the graphical results, the following viewpoints are obtained.

(1) The inhomogeneity of underground medium benefits to reduce the amplification effect of a circular canyon on the surface displacement amplitude.

(2) The inhomogeneity of underground medium makes the surface displacement of the wedge space more sensitive to dimensionless frequency and incident angle. That indicates the inhomogeneities of underground soils and rock masses have significant effect on wave propagation and ground motion.

(3) The wedge angle influences the amplification of the surface displacement amplitude of circular canyon. When $\gamma = 90^\circ$, the maximum amplification on the circular canyon to the surface displacement amplitude is about 1.4 times, when $\gamma = 120^\circ, 150^\circ$, it is about 1.6 times, and when $\gamma = 210^\circ$, it is about 2.7 times.

ACKNOWLEDGEMENTS

Each author contributed to this paper. ZY and XL wrote this paper, YS and GJ analysed the results, and MS and XF processed the data. This work is supported by the National Key Research and Development Program of China [grant number 2019YFC1509301], the National Natural Science Foundation of China [grant number 11872156], the Fundamental Research Funds for the Central Universities [grant number 3072020CFT0202], the State Key Laboratory of Mechanical Behavior and System Safety of Traffic Engineering Structures and the program for Innovative Research Team in China Earthquake Administration.

REFERENCE

Amornwongpaibun, A. & Lee, V.W., 2013. Scattering of anti-plane (SH) waves by a semi-elliptical hill: II—deep hill, *Soil Dyn. Earthq. Eng*., **52,** 126–137.

Ba, Z.N. & Yin, X., 2016. Wave scattering of complex local sites in a layered half-space by using a multidomain IBEM: incident plane SH waves, *Geophys. J. Int.,* **205,** 1382–1405.

Boore, D.M., 1972. A note on the effect of simple topography on seismic SH waves, *Bull. seism. Soc. Am.,* **62,** 275–284.

Chang, K.H., Tsaur, D.H. & Wang, J.H., 2013. Scattering of SH waves by a circular sectorial canyon, *Geophys. J. Int.,* **195,** 532–543.

Delepine, N. & Semblat, J.F., 2012. Site effects in an alpine valley with strong velocity gradient: interest and limitations of the 'classical' BEM, *Soil Dyn. Earthq. Eng*., **38,** 15–24.

Jiang, G.X.X., Yang, Z.L., Sun, C., Sun, B.T. & Yang, Y., 2018. Dynamic response of a circular inclusion embedded in inhomogeneous half-space, *Arch. Appl. Mech.,* **88,**1791–1803.

Larose, E. *et al.*, 2015. Environmental seismology: what can we learn on earth surface processes with ambient noise, *J. Appl. Gerontol.,* **116,** 62–74.

Lee, V.W. & Sherif, R.I., 1996. Diffraction around circular canyon in elastic wedge space by plane SH-waves, *J. Eng. Mech.,* **122,** 539–544.

Liu, G., Chen, H.T., Liu, D.K. & Khoo, B.C., 2010. Surface motion of a half-space with triangular and semicircular hills under incident SH waves, *Bull. seism. Soc. Am.,* **100,** 1306–1319.

Liu, Q.J., Zhao, M.J. & Zhang, C., 2014. Antiplane scattering of SH waves by a circular cavity in an exponentially graded half space, *Int. J. Eng. Sci.,* **78,** 61–72.

Liu, Q.J., Wu, Z.Y. & Lee, V.W., 2019. Scattering and reflection of SH waves around a slope on an elastic wedged space, *Earthq. Eng. Eng. Vib.,* **18,** 255–266.

Manolis, G.D. & Dineva, P.S., 2015. Elastic waves in continuous and discontinuous geological media by boundary integral equation methods: a review, *Soil Dyn. Earthq. Eng,* **70,** 11–29.

Marco, M., Simone, B. & Sara, L., 2014. Overview of topographic effects based on experimental observations: meaning, causes and possible interpretations, *Geophys. J. Int.,* **180,** 1537–1550.

Motosaka, M. & Mitsuji, K., 2012. Building damage during the 2011 off the Pacific coast of Tohoku Earthquake, *Soils Found*., **52,** 929–944.

Sanchez-Sesma, F.J., 1985. Diffraction of elastic SH-waves in wedges, *Bull. seism. Soc. Am.,* **75**(5), 1435–1446.

Trifunac, M.D., 1973. Scattering of plane SH waves by a semi-cylindrical canyon, *Earthq. Eng. Struct. Dyn.,* **1,** 267–281.

Tsaur, D.H. & Chang, K.H., 2008. An analytical approach for the scattering of SH waves by a symmetrical V-shaped canyon: shallow case, *Geophys. J. Int.,* **174,** 255–264.

Tsaur, D.H., Chang, K.H. & Hsu, M.S., 2018. Ground motions around a deep semielliptic canyon with a horizontal edge subjected to incident plane SH waves, *J. Seismol*., **22,** 1579–1593.

Víctor, H.A., Francisco, J.V. & Juan, D.J., 2017. Efficient solution for the diffraction of elastic SH waves by a wedge: Performance of various exact, asymptotic and simplified solutions, *Soil Dyn. Earthq. Eng*., **95,** 9–16.

Wong, H.L. & Trifunac, M.D., 1974. Scattering of plane SH waves by a semi-elliptical canyon, *Earthq. Eng. Struct. Dyn.,* **3,** 157–169.

Yang, Z.L., Song, Y.Q., Li, X.Z., Jiang, G.X.X. & Yang, Y., 2020. Scattering of plane SH waves by an isosceles trapezoidal hill, *Wave Motion,* **92,** 102415.

Yuan, X.M. & Men, F.L., 1992. Scattering of plane SH waves by a semi-cylindrical hill, *Earthq. Eng. Struct. Dyn.,* **21,** 1091–1098.

Zhang, C., Liu, Q.J. & Deng, P., 2015. Antiplane scattering of SH waves by a trapezoidal valley with a circular-arc alluvium in an elastic half space, *J. Earthq. Tsunami,* **9,** 1550008–1-1550008-23.

Zhang, N., Gao, Y.F. & Pak, R.Y.S., 2017. Soil and topographic effects on ground motion of a surficially inhomogeneous semi-cylindrical canyon under oblique incident SH waves, *Soil Dyn. Earthq. Eng*., **95,** 17–28.

Zhang, N., Zhang, Y. & Gao, Y.F., 2019a. An exact solution for SH-wave scattering by a radially multi-layered inhomogeneous semi-cylindrical canyon, *Geophys. J. Int.,* **217**(2), 1232–1260.

Zhang, N., Zhang, Y., Gao, Y.F., Pak, R.Y.S. & Yang, J., 2019b. Site amplification effects of a radially multi-layered semi-cylindrical canyon on seismic response of an earth and rockfill dam, *Soil Dyn. Earthq. Eng*., **116**(1), 145–163.